International Journal of Engineering Science 49 (2011) 561–575

Contents lists available at ScienceDirect

International Journal of Engineering Science

journal homepage: www.elsevier.com/locate/ijengsci

Multicoated elliptic fibrous composites of piezoelectric and piezomagnetic phases

Hsin-Yi Kuo

Department of Civil Engineering, National Chiao Tung University, Hsinchu 30010, Taiwan

ARTICLE INFO

Article history:
Received 8 December 2010
Received in revised form 28 January 2011
Accepted 17 February 2011
Available online 12 March 2011

Keywords:
Magnetoelectricity
Piezoelectric
Piezomagnetic
Elliptic fibrous composite
Multicoated

ABSTRACT

A theoretical framework is developed to investigate the magnetoelectroelastic potential in a multicoated elliptic fibrous composite with piezoelectric and piezomagnetic phases. We generalize the classic work of Rayleigh (1892) to obtain the electrostatic potential in ordered conductive composites and its extension to a disordered system (Kuo, 2010; Kuo & Chen, 2008) to the current coupled magnetoelectroelastic multicoated elliptic composites. We combine the methods of complex potentials with a re-expansion formulae and the generalized Rayleigh's formulation to obtain a complete solution of the multi-field many-inclusion problem. It is shown that the coefficients of field expansions can be written in the form of an infinite set of linear algebraic equations. Numerical results are presented for several configurations. We use this method to study $BaTiO_3$–$CoFe_2O_4$ composites and find that, with appropriate coating, the effective magnetoelectric voltage coefficient can be enhanced with one order of magnitude compared to their non-coating counterpart.

1. Introduction

Magnetoelectric materials, which induce the polarization by a magnetic field, or conversely induce the magnetization by an electric field, have been the focus of research due to their varieties of microstructural phenomena and macroscopic properties. These make them promising for a wide range of applications, such as four-state memories, magnetic field sensors, and magnetically controlled opto-electric devices (Eerenstein, Mathur, & Scott, 2006; Nan, Bichurin, Dong, Viehland, & Srinivasan, 2008). The study of magneto–electric coupling can be traced back to 1957 when Landau and Lifshitz (1984) showed the possibility of the coupling between the electric and magnetic fields in a substance with a certain magnetic symmetry class. This was subsequently experimentally confirmed in a single crystal Cr_2O_3 by Astrov (1960) and by Rado and Folen (1961) over 50 years ago. However, this coupling is weak in single phase materials, and thus has motivated the study of composites of piezoelectric and piezomagnetic media. The basic idea is to couple a piezoelectric and a piezomagnetic material using strain: an applied electric field creates a strain in the piezoelectric material which in turn induces a deformation in the piezomagnetic material, resulting in a magnetic field.

A number of micromechanical models hence were proposed to predict the effective moduli of multiferroic composites. For instance, Green's function approach was used by Nan (1994) and Huang and Kuo (1997) to study a fibrous composite consisting of Barium Titanate and Cobalt Ferrite. For such transversely isotropic fibrous composites, Benveniste (1995) derived exact connections among effective magnetoelectroelastic moduli based on a formalism discovered by Milgrom and Shtrikman (1989). Particulate composites were investigated by Harshé, Dougherty, and Newnham (1993) using a cubic model, while a homogenization micromechanical method was employed by Aboudi (2001). Eshelby's equivalent inclusion approach and the mean field Mori–Tanaka model have been generalized to multiferroic composites by Li and Dunn

E-mail address: hykuo@mail.nctu.edu.tw

0020-7225/$ - see front matter © 2011 Elsevier Ltd. All rights reserved.
doi:10.1016/j.ijengsci.2011.02.002

(1998a, 1998b), Huang (1998), Li (2000), Wu and Huang (2000) and Srinivas et al. (2006). A two-scale asymptotic homogenization theory was adopted by Camacho-Montes, Sabina, Bravo-Castillero, Guinovart-Díaz, and Rodríguez-Ramos (2009) on the magnetoelectric coupling and cross-property connections in a two-phase multiferroic composite. For a good overview of the subject, the reader is referred to the review article by Nan et al. (2008).

In a classic work, Lord Rayleigh computed the electrostatic potential for a conducting composite consisting of a periodic array of cylindrical or spherical inclusions. This was extended to arbitrary arrangements by Kuo and Chen (2008) and to elliptic cylinders by Kuo (2010). These works concern single fields. Later, Kuo and Bhattacharya (submitted for publication) generalized this methodology to electrostatic, magnetostatic and mechanical coupled fields. In this paper, we extend this Rayleigh's formulation further to a multiferroic composite consisting of elliptic cylinders, specifically multicoated ellipses.

Coating plays an important role in high-temperature systems and in various engineering applications. For instance, to reduce heat or stress concentration along the interface, interphase layers between the inclusions and the matrix are often introduced to act as thermal barrier. Graded materials can also be more damage-resistant than their conventional homogeneous counterpart (Suresh, 2001). Such interphase layer may have constant properties or spatially varying properties. Research into graded multiferroics has primarily been confined to bilayer and multilayer structures. Among them, piezoelectric or piezomagnetic coefficients are assumed linear variation in the thickness direction by Chen and Lee (2003), Petrov, Srinivasan, and Galkina (2008) and Petrov and Srinivasan (2008), while exponentially graded assumption is adopted by Pan and Han (2005) and Wang et al. (2009). To our knowledge, the subject of piezoelectric/piezomagnetic fibrous composites with multicoated elliptic cylinders has not been examined in the literature before.

The plan of this article is organized as follows. First we consider a composite medium made of piezoelectric and piezomagnetic phases arranged in a microstructure consisting of parallel elliptic cylinders in a matrix in Section 2. The phases are transversely isotropic and under anti-plane shear with in-plane electromagnetic fields. In this situation, the fields are decoupled in the interior of every phase, and the coupling between the fields occurs only through the interface conditions (Kuo & Bhattacharya, submitted for publication). We exploit this in Section 2.2 to obtain a representation of the solution. The basic idea is to follow Kuo (2010) and expand each field in each medium in a series. We consider periodic arrays in Section 2.3. In Section 3 we consider the case of multicoated elliptic cylinders. We show that a (6×6) array alone can mathematically simulate the effects of multiple coatings. We obtain effective properties in Section 4, and significantly show that the macroscopic properties depend solely on a single expansion coefficient (amongst the infinite). This methodology is illustrated in Section 5 using composites of $BaTiO_3$ and $CoFe_2O_4$. We choose this material pair for its practical potential and also because it enables comparison with previous work. We observe that the composite medium has a non-trivial magnetoelectric coupling even through the individual components do not. Further, we show that the ME coefficient can be enhanced with an order of magnitude if the $BaTiO_3$ fiber is coated with Terfenol-D.

2. Multiple elliptic cylinders

2.1. Basic formulations

Let us consider an infinite medium $\mathbb{R}^3$ containing N arbitrarily distributed, parallel and separated elliptic cylinders. The domain of the pth elliptic cylinder is denoted V_p, $p = 1,2,\ldots,N$, and the remaining matrix is denoted Ω_m. We assume that the cylinders and the matrix are made of distinct phases. Further, we assume that each phase is either piezoelectric or piezomagnetic with transversely isotropic symmetry (i.e. has 6 mm symmetry) about the fiber axes. We introduce a Cartesian coordinate system positioned at a selected point O of the plane with the x- and y-axes in the plane of the cross-section and z- along the axes of the cylinders (Fig. 1). The centroids of the pth elliptic cylinders are designated as O_p, with O_px_p and O_py_p axes are directed along the major and minor axes of the ellipse. Each of ellipse has the major and minor semi-axis, $l_x^{(p)}$ and $l_y^{(p)}$, and the inter-foci distance is $2d_p$, where $d_p^2 = l_x^{(p)2} - l_y^{(p)2}$. The ellipses are well separated so that any two inclusions will not get in touch with each other.

Let the composite be subjected to the anti-plane shear strain $\bar{\varepsilon}_{zx}$, $\bar{\varepsilon}_{zy}$, the in-plane electric fields $\overline{E}_x$, $\overline{E}_y$, and the magnetic fields $\overline{H}_x$, $\overline{H}_y$ at infinity. Thus the heterogeneous material is in a state of anti-plane shear problem (Benveniste, 1995; Chen, 1993; Kuo & Bhattacharya, submitted for publication) and can be described by

$$\begin{aligned} &u_x = u_y = 0, \quad u_z = w(x,y), \\ &\varphi = \varphi(x,y), \\ &\psi = \psi(x,y), \end{aligned} \tag{2.1}$$

where u_x, u_y, u_z are the mechanical displacements along the x-, y-, and z-axes, and φ and $\psi$are the electric and magnetic potentials, respectively.

The constitutive laws of the constituents for the non-vanishing fields become

$$\begin{pmatrix} \sigma_{zj} \\ D_j \\ B_j \end{pmatrix} = \begin{pmatrix} C_{44} & e_{15} & q_{15} \\ e_{15} & -\kappa_{11} & -\lambda_{11} \\ q_{15} & -\lambda_{11} & -\mu_{11} \end{pmatrix} \begin{pmatrix} \varepsilon_{zj} \\ -E_j \\ -H_j \end{pmatrix}, \tag{2.2}$$

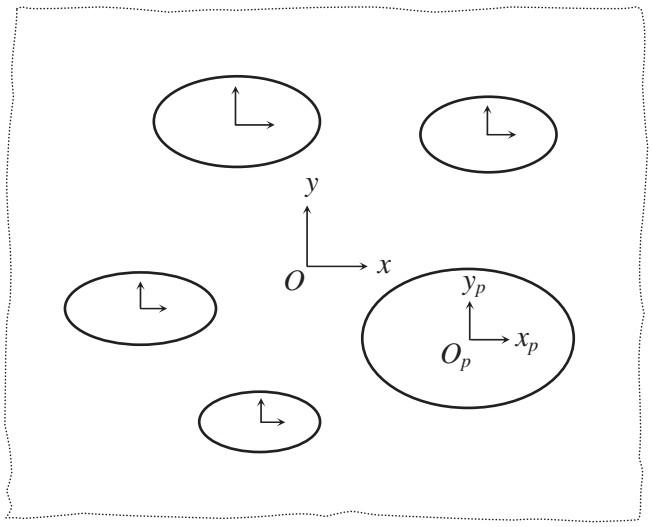

Fig. 1. The cross-section of the fiber composite.

where j denotes the component x,y. We can write this compactly as

$$\Sigma_j^U = L_{UV} Z_j^V, \quad U,V = w,\varphi,\psi, \quad j = x,y, \tag{2.3}$$

where

$$\mathbf{\Sigma}_j = \begin{pmatrix} \sigma_{zj} \\ D_j \\ B_j \end{pmatrix}, \quad \mathbf{L} = \begin{pmatrix} C_{44} & e_{15} & q_{15} \\ e_{15} & -\kappa_{11} & -\lambda_{11} \\ q_{15} & -\lambda_{11} & -\mu_{11} \end{pmatrix}, \quad \mathbf{Z}_j = \begin{pmatrix} \varepsilon_{zj} \\ -E_j \\ -H_j \end{pmatrix}. \tag{2.4}$$

Here $\sigma_{zj}, D_j, B_j, \varepsilon_{zj}, E_j$ and H_j are the stress, electric displacement, magnetic flux, strain, electric field, and the magnetic field, respectively. $C_{44}, \kappa_{11}, \mu_{11}$ and λ_{11} are the elastic modulus, dielectric permittivity, magnetic permeability and magnetoelectric coefficients. The shear strains ε_{zx} and ε_{zy}, in-plane electric fields E_x and E_y, and in-plane magnetic fields H_x and H_y can be derived from the gradient of elastic displacement, electric potential, and magnetic potential as follows:

$$\begin{aligned} &\varepsilon_{zx} = \frac{\partial w}{\partial x}, \quad \varepsilon_{zy} = \frac{\partial w}{\partial y}, \\ &E_x = -\frac{\partial \varphi}{\partial x}, \quad E_y = -\frac{\partial \varphi}{\partial y}, \\ &H_x = -\frac{\partial \psi}{\partial x}, \quad H_y = -\frac{\partial \psi}{\partial y}. \end{aligned} \tag{2.5}$$

Further, the equilibrium equations, in the absence of body force, electric charge density and electric current density, are given by

$$\begin{aligned} &\frac{\partial \sigma_{zx}}{\partial x} + \frac{\partial \sigma_{zy}}{\partial y} = 0, \\ &\frac{\partial D_x}{\partial x} + \frac{\partial D_y}{\partial y} = 0, \\ &\frac{\partial B_x}{\partial x} + \frac{\partial B_y}{\partial y} = 0. \end{aligned} \tag{2.6}$$

Substitution of Eq. (2.3) into Eq. (2.6) yields

$$\begin{aligned} &C_{44}\nabla^2 w + e_{15}\nabla^2 \varphi + q_{15}\nabla^2 \psi = 0, \\ &e_{15}\nabla^2 w - \kappa_{11}\nabla^2 \varphi - \lambda_{11}\nabla^2 \psi = 0, \\ &q_{15}\nabla^2 w - \lambda_{11}\nabla^2 \varphi - \mu_{11}\nabla^2 \psi = 0, \end{aligned} \tag{2.7}$$

where $\nabla^2 = \partial^2/\partial x^2 + \partial^2/\partial y^2$ represents the two-dimensional Laplace operator for the variable x and y. Since $\mathbf{L}$ is a nonsingular matrix, generically we can completely decouple (2.7) into three independent Laplace equations,

$$\nabla^2 w = 0, \quad \nabla^2 \varphi = 0, \quad \nabla^2 \psi = 0 \tag{2.8}$$

in the interior of each phase.

In addition to these differential equations, we have to use interface conditions. We assume that the interfaces are perfectly bonded, and therefore the fields satisfy

$$[\![\mathbf{Z}_j t_j]\!] = \mathbf{0}, \quad [\![[\boldsymbol{\Sigma}_j n_j]\!] = [\![(\mathbf{L}\mathbf{Z}_j) n_j]\!] = \mathbf{0} \tag{2.9}$$

where $[\![\cdot]\!]$ denotes the jump in some quantity across the interface, t_j is the unit tangent to the interface and n_j is the unit outward normal to the interface, and the repeated index j denotes summing over the components x,y. Since $\mathbf{L}$ is different in each phase, the fields w, φ and ψ are generally coupled by the interface equations.

2.2. Representation of the solution

We start by considering the case that the cylinders are homogeneous. We showed above that the fields are decoupled in the interior of every phase, but are coupled at the interfaces. Therefore, we may follow Kuo (2010) and use a series expansion for each field in the interior of each phase and then obtain the coefficients by enforcing the interface and boundary conditions.

Since w, φ and ψ are harmonic, we can construct an analytic function $\Phi(z) = U(z) + \mathrm{i}U^*(z)$, of the complex variable $z = x + \mathrm{i}y$, where U^* is the conjugate harmonic function, related to U by the Cauchy-Riemann equation

$$\frac{\partial U}{\partial x} = \frac{\partial U^*}{\partial y}, \quad \frac{\partial U}{\partial y} = -\frac{\partial U^*}{\partial x}, \quad U = w, \varphi, \psi. \tag{2.10}$$

Further, the shape of the cross section of the cylinders defines elliptic coordinates: ($\mu > 0, -\pi < \theta \leqslant \pi$)

$$z = x + \mathrm{i}y = d\cosh\omega = d\cosh(\mu + \mathrm{i}\theta) \tag{2.11}$$

are the most appropriate system for the solution of Laplace's equation.

We now consider a situation where the composite is subjected to a macroscopically uniaxial loading

$$w_{\text{ext}} = \bar{\varepsilon}_{zx} x, \quad \varphi_{\text{ext}} = -\overline{E}_x x, \quad \psi_{\text{ext}} = -\overline{H}_x x, \tag{2.12}$$

for constant $\bar{\varepsilon}_{zx}, \overline{E}_x$ and $\overline{H}_x$. We may rewrite this in short as

$$\Phi_{\text{ext}} = \Gamma^{\Phi} z, \tag{2.13}$$

where Φ represents the appropriate field – the anti-plane deformation w, electric potential φ, or magnetic potential ψ – and $\Gamma^{\Phi} = \Gamma^{\Phi}_R + \mathrm{i}\Gamma^{\Phi}_I$ the corresponding applied field – $\bar{\varepsilon}_{zx}$, $-\overline{E}_x$ or $-\overline{H}_x$.

We rewrite the governing equation, Eq. (2.8), in elliptic coordinates (μ, θ),

$$\nabla^2 \Phi = \frac{1}{d^2(\cosh^2\mu - \cos^2\theta)}\left(\frac{\partial^2 \Phi}{\partial \mu^2} + \frac{\partial^2 \Phi}{\partial \theta^2}\right) = 0. \tag{2.14}$$

The potential field for the pth elliptic cylinder and its surrounding matrix can be expanded with respect to its centroid O_p as

$$\Phi_i^{(p)}(z_p) = \sum_{n=-\infty}^{\infty} C_n^{\Phi(p)} e^{-n\omega_p}, \quad C_n^{\Phi(p)} = C_{-n}^{\Phi(p)} \tag{2.15}$$

for the inclusion, and

$$\Phi_m^{(p)}(z_p) = \sum_{n=-\infty}^{\infty} A_n^{\Phi(p)} e^{-n\omega_p} + \sum_{n=1}^{\infty} B_n^{\Phi(p)} e^{-n\omega_p}, \quad A_n^{\Phi(p)} = A_{-n}^{\Phi(p)} \tag{2.16}$$

for the matrix. Here $\omega_p = \mu_p + \mathrm{i}\theta_p$ is the local elliptic coordinate centered at the origin of the pth ellipse, the subscripts i and m denote the inclusion and matrix, respectively. The coefficients $A_n^{\Phi(p)} = A_{nR}^{\Phi(p)} + \mathrm{i}A_{nI}^{\Phi(p)}$, $B_n^{\Phi(p)} = B_{nR}^{\Phi(p)} + \mathrm{i}B_{nI}^{\Phi(p)}$ and $C_n^{\Phi(p)} = C_{nR}^{\Phi(p)} + \mathrm{i}C_{nI}^{\Phi(p)}$ are some complex unknowns to be determined. The superscripts p appearing in (2.15) and (2.16) indicate that the fields are expanded with respect to the pth ellipse centroid.

We recall the interface conditions (2.9) which we rewrite as

$$\mathrm{Re}\Phi_i^{(p)}\Big|_{\partial V_p} = \mathrm{Re}\Phi_m^{(p)}\big|_{\partial V_p}, \quad (\boldsymbol{\Sigma}^{\Phi})_m^{(p)} \cdot \mathbf{n}_p\Big|_{\partial V_p} = (\boldsymbol{\Sigma}^{\Phi})_i^{(p)} \cdot \mathbf{n}_p\Big|_{\partial V_p} \tag{2.17}$$

where

$$\boldsymbol{\Sigma}^{w} = (\sigma_{zx}, \sigma_{zy}), \quad \boldsymbol{\Sigma}^{\varphi} = (D_x, D_y), \quad \boldsymbol{\Sigma}^{\psi} = (B_x, B_y), \tag{2.18}$$

$\partial V_p : \mu_p = a_p$ denotes the interface between the matrix and the pth elliptic cylinder, and $\mathbf{n}_p$ is the unit outward normal of the interface ∂V_p.

Using the orthogonality properties of trigonometric functions, the interface conditions (2.17) provide

$$\mathbf{a}_{n\Lambda}^{(p)} = \mathbf{T}_{an\Lambda}^{(p)}\mathbf{b}_{n\Lambda}^{(p)}, \quad \mathbf{c}_{n\Lambda}^{(p)} = \mathbf{T}_{cn\Lambda}^{(p)}\mathbf{b}_{n\Lambda}^{(p)}, \tag{2.19}$$

and $A_0^{\Phi(p)} = C_0^{\Phi(p)}$, where

$$\mathbf{a}_{n\Lambda}^{(p)} = \begin{pmatrix} A_{n\Lambda}^{w(p)} \\ A_{n\Lambda}^{\varphi(p)} \\ A_{n\Lambda}^{\psi(p)} \end{pmatrix}, \quad \mathbf{b}_{n\Lambda}^{(p)} = \begin{pmatrix} B_{n\Lambda}^{w(p)} \\ B_{n\Lambda}^{\varphi(p)} \\ B_{n\Lambda}^{\psi(p)} \end{pmatrix}, \quad \mathbf{c}_{n\Lambda}^{(p)} = \begin{pmatrix} C_{n\Lambda}^{w(p)} \\ C_{n\Lambda}^{\varphi(p)} \\ C_{n\Lambda}^{\psi(p)} \end{pmatrix}, \tag{2.20}$$

$$\begin{aligned} \mathbf{T}_{anR}^{(p)} &= \left(\mathbf{L}^{(m)} - \mathbf{L}^{(p)}\right)^{-1}\left(\cosh na_p\mathbf{L}^{(m)} + \sinh na_p\mathbf{L}^{(p)}\right)\frac{e^{-na_p}}{\sinh 2na_p}, \\ \mathbf{T}_{anI}^{(p)} &= \left(\mathbf{L}^{(m)} - \mathbf{L}^{(p)}\right)^{-1}\left(\sinh na_p\mathbf{L}^{(m)} + \cosh na_p\mathbf{L}^{(p)}\right)\frac{-e^{-na_p}}{\sinh 2na_p}, \\ \mathbf{T}_{cnR}^{(p)} &= \mathbf{T}_{anR}^{(p)} + \frac{e^{-na_p}}{2\cosh na_p}\mathbf{I}, \quad \mathbf{T}_{cnI}^{(p)} = \mathbf{T}_{anI}^{(p)} - \frac{e^{-na_p}}{2\sinh na_p}\mathbf{I}, \end{aligned} \tag{2.21}$$

Λ represents R, the real part, or I, the imaginary part of the coefficients, and $\mathbf{I}$ is the 3×3 identity tensor.

We now need to relate the solutions to the applied boundary conditions. We do so by applying the Green's second identity (Arfken & Weber, 2001) to the matrix domain Ω_m. This gives

$$\int_{\Omega_m}\left[G(\mathbf{x};\mathbf{x}')\nabla'^2\Phi_m(\mathbf{x}') - \Phi_m(\mathbf{x}')\nabla'^2G(\mathbf{x};\mathbf{x}')\right]dA' = \int_{\partial\Omega_m}\left[G(\mathbf{x};\mathbf{x}')\nabla'\Phi_m(\mathbf{x}') - \Phi_m(\mathbf{x}')\nabla'G(\mathbf{x};\mathbf{x}')\right]\cdot\boldsymbol{n}'\,ds', \tag{2.22}$$

where the prime $'$ denotes the operation in reference to the $\mathbf{x}'$ coordinate, $\boldsymbol{n}'$ is the outward unit normal to the matrix's boundary $\partial\Omega_m$, dA' represents the area element for the $\mathbf{x}'$ coordinate, ds' is the differential arc length. Here $G(\mathbf{x};\mathbf{x}')$ is the free-space Green's function for Laplace operator satisfying $\nabla^2G(\mathbf{x};\mathbf{x}') = -\delta(\mathbf{x}-\mathbf{x}')$, where $\delta(\mathbf{x}-\mathbf{x}')$ is the Dirac-delta function. Following the procedure in Kuo (2010), it can be shown that Eq. (2.22) yields

$$\Phi_m(z) = \Phi_{\text{ext}}(z) + \sum_{l=1}^{N}\sum_{n=1}^{\infty}B_m^{\Phi(l)}e^{-n\omega_l}. \tag{2.23}$$

This is the consistency equation which relates the external applied fields to the local potential expansions. Note that the field identity (2.23) is written based on different coordinates.

To proceed, we shift the origin of the expansions (2.23) to a fixed point, say Z_p, the centroid of the pth ellipse, by expanding the term $e^{-m\omega_l}$ as Kushch, Shmegera, and Buryachenko (2005)

$$e^{-n\omega_l} = \sum_{m=-\infty}^{\infty}\eta_{nm}^{lp}e^{-m\omega_p}, \tag{2.24}$$

with

$$\eta_{nm}^{lp} = (-1)^m n\left(\frac{d_l}{d_{lp}}\right)^n\sum_{s=0}^{\infty}\nu_{lp}^{-(n+m+2s)}\sum_{t=0}^{s}\frac{(-1)^{s-t}}{(s-t)!}\left(\frac{d_p}{d_{lp}}\right)^{m+2t}M_{nmt}(d_l,d_p)\frac{(n+m+t+s-1)!}{(s-t)!}, \tag{2.25}$$

where $d_{lp} \equiv d_l + d_p$, $\nu_{lp} \equiv Z_{lp}/d_{lp} + \sqrt{(Z_{lp}/d_{lp})^2 - 1}$ and

$$M_{nmt}(d_l,d_p) = \sum_{k=0}^{t}\frac{(d_l/d_p)^{2k}}{k!(t-k)!(k+n)!(m+t-k)!}. \tag{2.26}$$

Introducing (2.24) into (2.23), we have the expansion

$$\Phi_{m,near}^{(p)}(z) = \Gamma^{\Phi}Z_p + \sum_{n=-\infty}^{\infty}\left(B_n^{\Phi(p)} + b_n^{\Phi(p)}\right)e^{-m\omega_p}, \tag{2.27}$$

where

$$b_n^{\Phi(p)} = \Gamma^{\Phi}\frac{d_p}{2}\delta_{n,\pm1} + \sum_{l\neq p}^{N}\sum_{m=1}^{\infty}B_m^{\Phi(l)}\eta_{mn}^{lp} \tag{2.28}$$

valid for the domain within an ellipse centered in Z_p with inter-foci distance $2d_{lp}$ and passing the pole of lth elliptic coordinate systems closest to Z_p (Kushch et al., 2005). Further, since z lies in the matrix domain, Eqs. (2.27) and (2.16) should be identical. This provides the condition

$$\sum_{n=-\infty}^{\infty}A_n^{\Phi(p)}e^{-n\omega_p} = \Gamma^{\Phi}Z_p + \sum_{n=-\infty}^{\infty}b_n^{\Phi(p)}e^{-n\omega_p}. \tag{2.29}$$

Taking the real part and the imaginary part of (2.29), we find the two conditions

$$A_{nR}^{\Phi(p)} = (\Gamma_R^{\Phi}\mathrm{Re}Z_p - \Gamma_I^{\Phi}\mathrm{Im}Z_p)\delta_{n,0} + b_{nR}^{\Phi(p)}, \tag{2.30}$$

and

$$A_{nI}^{\Phi(p)} = (\Gamma_I^{\Phi}\mathrm{Re}Z_p + \Gamma_R^{\Phi}\mathrm{Im}Z_p)\delta_{n,0} + b_{nI}^{\Phi(p)}. \tag{2.31}$$

Eqs. (2.30), (2.31) and $(2.19)_1$ constitute an infinite set of linear algebraic equations. Upon appropriate truncations of the expansions terms, we can determine the expansion coefficients $A_n^{\Phi(p)}$, $B_n^{\Phi(p)}$, $C_n^{\Phi(p)}$. Here we make one further remark.

Remark. The essential step of the framework is to establish the generalized Rayleigh's identities, (2.30) and (2.31). We observe, however, that the derivation of the identities is independent of inclusions' expansions. In other words, these identities can be applicable to inclusions with inhomogeneous constituents provided that the admissible fields in the inclusions and the transition relations, similar to (2.19) can be constructed.

2.3. Periodic arrays

The analysis carried out in the previous section for the arbitrary system with a finite number of cylinders may also be adapted for the case of a periodic array of cylinders. Here we concentrate on the rectangular lattice, and we sketch the outline of the derivation focussing on the differences from the previous situation.

Let us first introduce a Cartesian coordinate system (x,y) positioned at the centroid O of one of the ellipses in a rectangular array, as shown in Fig. 2. The sides of the rectangular cell parallel to the x and y coordinates are, respectively, denoted by α and β. The elliptic cylinders are of the same orientation, elliptic radius $\mu = a$ and inter-foci distance $2d$. Uniform intensities $\overline{E}_x$ and $\overline{H}_x$ are applied along the positive x axis, and an anti-plane shear deformation $\overline{\varepsilon}_{zx}$ is applied out of the xy plane. In terms of elliptic coordinates, the general solution has the admissible form

$$\Phi_i = \sum_{n=-\infty}^{\infty} C_n^{\Phi} e^{-n\omega}, \quad C_n^{\Phi} = C_{-n}^{\Phi} \tag{2.32}$$

for $\mu < a$, and

$$\Phi_m = \sum_{n=-\infty}^{\infty} A_n^{\Phi} e^{-n\omega} + \sum_{n=1}^{\infty} B_n^{\Phi} e^{-n\omega}, \quad A_n^{\Phi} = A_{-n}^{\Phi}, \tag{2.33}$$

for $\mu > a$. The coefficients A_n^{Φ}, B_n^{Φ}, and C_n^{Φ} are unknown complex constants to be determined from the interface and boundary conditions.

Analogous to (2.19), the continuity conditions at the interface will give constraints (2.19) between the coefficients. Next, imposing the periodicity conditions analogous to the boundary condition we did to derive (2.30) and (2.31), lead to generalized Rayleigh's identities

$$A_{n\Lambda}^{\Phi} = b_{n\Lambda}^{\Phi}, \quad \Lambda = R, I. \tag{2.34}$$

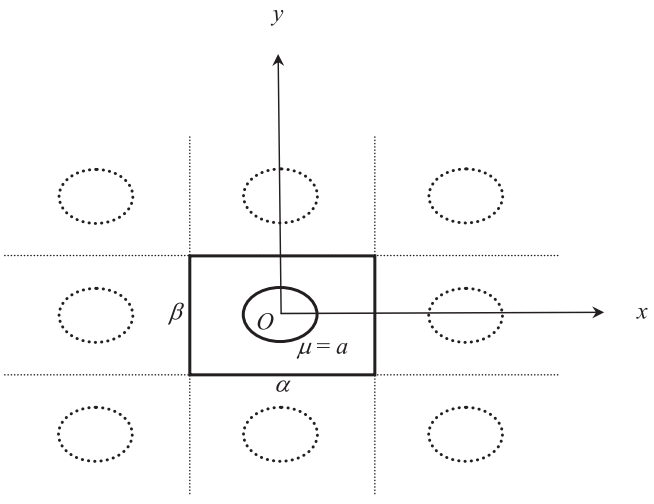

Fig. 2. A schematic representation of a unit cell.

Here the quantities

$$b_n^{\Phi} = -\Gamma^{\Phi}\frac{d}{2}\delta_{n,\pm 1} + \sum_{m=1}^{\infty} B_m^{\Phi}\sum_{l\neq o}^{\infty}\eta_{mn}^{lo}, \tag{2.35}$$

$$\sum_{l\neq o}^{\infty}\eta_{mn}^{lo} = (-1)^m n\sum_{t=0}^{\infty}\left(\frac{d}{2}\right)^{n+m+2t} M_{nmt}(d,d)(n+m+2t-1)!S_{n+m+2t}, \tag{2.36}$$

where $M_{nmt}(\cdot)$ is defined in (2.26), and

$$S_m = \sum_{l\neq o} Z_l^{-m}, \tag{2.37}$$

are the lattice sums characterizing the geometry of the periodic structure, and Z_l is the centroid of the lth cylinder when measured in the complex plane centered at the central point O. The index l runs over all cylinders' centers underlying the periodic array except the central one. Previous studies (Rayleigh, 1892) have reported that the sum S_2 is conditionally convergent and its value depends upon the shape of the exterior boundary of the array. A list of S_2 for different values of α/β can be found in Nicrovici and McPhedran (1996).

Eqs. (2.34) and $(2.19)_1$ constitute an infinite set of linear algebraic equations. Upon appropriate truncations of the expansion terms at a finite order M, we can determine the expansion coefficients A_n^{Φ}, B_n^{Φ}, and C_n^{Φ}.

3. Confocally multicoated elliptic cylinders

From the previous remark, we now consider that the inclusions are confocally multicoated elliptic cylinders with the outer elliptic radius $a_p^{(1)}$, $p = 1,2,\ldots,N$, where N is the number of inclusions. We denote the matrix as phase 0, with transversely isotropic material parameters $C_{44}^{(0)}$, $e_{15}^{(0)}$, $q_{15}^{(0)}$, $\kappa_{11}^{(0)}$, $\mu_{11}^{(0)}$ and $\lambda_{11}^{(0)}$. The multicoated cylinder consists of a core, with radius $\mu_p = a_p^{(\mathcal{M})}$, surrounded by $(\mathcal{M}-1)$ layers of coating. The jth layer of the coatings occupies the annulus $V_p^{(j)}: a_p^{(j+1)} \leqslant \mu_p \leqslant a_p^{(j)}$, $j = 1,2,\ldots,\mathcal{M}$, in which $V_p = V_p^{(1)} \cup V_p^{(2)} \cup \cdots \cup V_p^{(\mathcal{M})}$. Here the innermost core is solid so that we have $a_p^{(\mathcal{M}+1)} = 0$. We assume that the material properties of jth constituent layer of the pth multicoated cylinder are $C_{44}^{(p,j)}$, $e_{15}^{(p,j)}$, $q_{15}^{(p,j)}$, $\kappa_{11}^{(p,j)}$, $\mu_{11}^{(p,j)}$ and $\lambda_{11}^{(p,j)}$.

The admissible potentials in each constituent layer of the multicoated inclusion can be expressed as

$$\Phi^{(p,j)} = \sum_{n=-\infty}^{\infty} A_n^{\Phi(p,j)} e^{-n\omega_p} + \sum_{n=1}^{\infty} B_n^{\Phi(p,j)} e^{-n\omega_p}, \quad A_n^{\Phi(p,j)} = A_{-n}^{\Phi(p,j)}, \tag{3.1}$$

where $A_n^{\Phi(p,j)} = A_{nR}^{\Phi(p,j)} + \mathrm{i}A_{nI}^{\Phi(p,j)}$ and $B_n^{\Phi(p,j)} = B_{nR}^{\Phi(p,j)} + \mathrm{i}B_{nI}^{\Phi(p,j)}$ are unknown complex constants to be determined. Note that the potential at $\mu \to 0$ should be finite and thus we can set

$$B_n^{\Phi(p,\mathcal{M})} = 0. \tag{3.2}$$

We consider that the interfaces are perfectly bonded, the potential and the normal component of flux are continuous across the interfaces,

$$\begin{aligned} &\mathrm{Re}\Phi^{(p,j-1)}\Big|_{\mu_p = a_p^{(j)}} = \mathrm{Re}\Phi^{(p,j)}\Big|_{\mu_p = a_p^{(j)}}, \\ &\left(\boldsymbol{\Sigma}^{\Phi}\right)^{(p,j-1)}\cdot\mathbf{n}_p^{(j)}\Big|_{\mu_p = a_p^{(j)}} = \left(\boldsymbol{\Sigma}^{\Phi}\right)^{(p,j)}\cdot\mathbf{n}_p^{(j)}\Big|_{\mu_p = a_p^{(j)}}. \end{aligned} \tag{3.3}$$

These continuity conditions lead to

$$\begin{pmatrix} \mathbf{a}_{n\Lambda}^{(p,j-1)} \\ \mathbf{b}_{n\Lambda}^{(p,j-1)} \end{pmatrix} = \mathbf{k}_{n\Lambda}^{(p,j)} \begin{pmatrix} \mathbf{a}_{n\Lambda}^{(p,j)} \\ \mathbf{b}_{n\Lambda}^{(p,j)} \end{pmatrix}, \quad \Lambda = R, I, \quad j = 1,2,\ldots,\mathcal{M}, \tag{3.4}$$

where

$$\mathbf{a}_{n\Lambda}^{(p,j)} = \begin{pmatrix} A_{n\Lambda}^{w(p,j)} \\ A_{n\Lambda}^{\varphi(p,j)} \\ A_{n\Lambda}^{\psi(p,j)} \end{pmatrix}, \quad \mathbf{b}_{n\Lambda}^{(p,j)} = \begin{pmatrix} B_{n\Lambda}^{w(p,j)} \\ B_{n\Lambda}^{\varphi(p,j)} \\ B_{n\Lambda}^{\psi(p,j)} \end{pmatrix}, \tag{3.5}$$

$$\begin{aligned} \mathbf{k}_{nR}^{(p,j)} &\equiv \begin{pmatrix} 2\cosh na_p^{(j)}\mathbf{I} & e^{-na_p^{(j)}}\mathbf{I} \\ -2\sinh na_p^{(j)}\mathbf{L}^{(j-1)} & e^{-na_p^{(j)}}\mathbf{L}^{(j-1)} \end{pmatrix}^{-1} \begin{pmatrix} 2\cosh na_p^{(j)}\mathbf{I} & e^{-na_p^{(j)}}\mathbf{I} \\ -2\sinh na_p^{(j)}\mathbf{L}^{(j)} & e^{-na_p^{(j)}}\mathbf{L}^{(j)} \end{pmatrix}, \\ \mathbf{k}_{nI}^{(p,j)} &\equiv \begin{pmatrix} -2\sinh na_p^{(j)}\mathbf{I} & e^{-na_p^{(j)}}\mathbf{I} \\ 2\cosh na_p^{(j)}\mathbf{L}^{(j-1)} & e^{-na_p^{(j)}}\mathbf{L}^{(j-1)} \end{pmatrix}^{-1} \begin{pmatrix} -2\sinh na_p^{(j)}\mathbf{I} & e^{-na_p^{(j)}}\mathbf{I} \\ 2\cosh na_p^{(j)}\mathbf{L}^{(j)} & e^{-na_p^{(j)}}\mathbf{L}^{(j)} \end{pmatrix}, \end{aligned} \tag{3.6}$$

and $\mathbf{I}$ is the 3×3 identity matrix. Now, repeated use of (3.4) gives

$$\begin{pmatrix} \mathbf{a}_{n\Lambda}^{(p,0)} \\ \mathbf{b}_{n\Lambda}^{(p,0)} \end{pmatrix} = \mathbf{K}_{p\Lambda}^{(j,n)} \begin{pmatrix} \mathbf{a}_{n\Lambda}^{(p,j)} \\ \mathbf{b}_{n\Lambda}^{(p,j)} \end{pmatrix}, \quad j = 1, 2, \ldots, \mathcal{M}, \tag{3.7}$$

where

$$\mathbf{K}_{p\Lambda}^{(j,n)} \equiv \mathbf{k}_{n\Lambda}^{(p,1)} \mathbf{k}_{n\Lambda}^{(p,2)} \cdots \mathbf{k}_{n\Lambda}^{(p,j)}. \tag{3.8}$$

For $j = \mathcal{M}$, we have

$$\begin{pmatrix} \mathbf{a}_{n\Lambda}^{(p,0)} \\ \mathbf{b}_{n\Lambda}^{(p,0)} \end{pmatrix} = \mathbf{K}_{p\Lambda}^{(\mathcal{M},n)} \begin{pmatrix} \mathbf{a}_{n\Lambda}^{(p,\mathcal{M})} \\ \mathbf{b}_{n\Lambda}^{(p,\mathcal{M})} \end{pmatrix}. \tag{3.9}$$

Further, according to (3.2), (3.9), implies that

$$\mathbf{a}_{n\Lambda}^{(p,0)} = \left[\mathbf{K}_{p\Lambda}^{(\mathcal{M},n)}\right]_{11} \left[\mathbf{K}_{p\Lambda}^{(\mathcal{M},n)}\right]_{21}^{-1} \mathbf{b}_{n\Lambda}^{(p,0)}. \tag{3.10}$$

Here $[\mathbf{K}_{p\Lambda}^{(\mathcal{M},n)}]_{11}$ represents the upper-left (3×3) submatrix of $\mathbf{K}_{p\Lambda}^{(\mathcal{M},n)}$ and $[\mathbf{K}_{p\Lambda}^{(\mathcal{M},n)}]_{21}$ is the lower-left (3×3) submatrix of $\mathbf{K}_{p\Lambda}^{(\mathcal{M},n)}$. The formulation implies that the effect of the multiple coatings can be incorporated through a recurrence procedure and is solely represented by a (6×6) array alone. We mention that once we construct the admissible field (3.1) and the transition relation (3.4) in the inhomogneneous inclusions, we can follow the remaining generalized Rayleigh's framework proposed in previous section to determine the potential distribution.

4. Effective moduli

We are interested in the effective behavior for a situation where we have a large number of cylinders. The effective material properties are defined in terms averaged fields,

$$\langle \mathbf{\Sigma}_j \rangle \equiv \mathbf{L}_j^* \langle \mathbf{Z}_j \rangle, \quad \text{no summation}, \tag{4.1}$$

where the angular brackets denote the area averages over the representative volume element (unit cell in the case of periodic composites)

$$\langle \mathbf{\Sigma}_j \rangle = \frac{1}{V} \int_V \mathbf{\Sigma}_j d\mathbf{x}, \quad \langle \mathbf{Z}_j \rangle = \frac{1}{V} \int_V \mathbf{Z}_j d\mathbf{x}, \tag{4.2}$$

and $\mathbf{L}_j^*$ denotes the effective magnetoelectroelastic parameters of the composite. Note that since the microstructure is non-symmetric, the responses of the composite along x and y-axes are different:

$$\mathbf{L}_x^* = \begin{pmatrix} C_{55}^* & e_{15}^* & q_{15}^* \\ e_{15}^* & -\kappa_{11}^* & -\lambda_{11}^* \\ q_{15}^* & -\lambda_{11}^* & -\mu_{11}^* \end{pmatrix}, \quad \mathbf{L}_y^* = \begin{pmatrix} C_{44}^* & e_{24}^* & q_{24}^* \\ e_{24}^* & -\kappa_{22}^* & -\lambda_{22}^* \\ q_{24}^* & -\lambda_{22}^* & -\mu_{22}^* \end{pmatrix}. \tag{4.3}$$

Let the composite be subjected to uniform intensities $\bar{\varepsilon}_{zx}$, $-\overline{E}_x$, and $-\overline{H}_x$ along the positive x- axis. We can compute the average $\mathbf{Z}_x$ by noting that each component is a gradient and applying the divergence theorem. We obtain:

$$\langle Z_x^{\Phi} \rangle = \Gamma_R^{\Phi}. \tag{4.4}$$

Next, to find $\langle \Sigma_x^{\Phi} \rangle$, we again use the divergence theorem and the equilibrium condition (including the interface conditions) to obtain

$$\langle \Sigma_x^{\Phi} \rangle = \frac{1}{V} \int_V \Sigma_x^{\Phi} d\mathbf{x} = \frac{1}{V} \int_V \nabla \cdot (x \mathbf{\Sigma}^{\Phi}) d\mathbf{x} = \frac{1}{V} \int_{\partial V} x (\mathbf{\Sigma}^{\Phi})_m \cdot \mathbf{n}\, ds, \tag{4.5}$$

where $\mathbf{\Sigma}^{\Phi}$ is defined in (2.18). We then use the expansions (2.16) for the fields to obtain

$$\frac{1}{V} \int_{\partial V} x (\mathbf{Z}^{\Phi})_m \cdot \mathbf{n}\, ds = \Gamma_R^{\Phi} - \frac{\pi d B_{1R}^{\Phi}}{\alpha\beta}, \tag{4.6}$$

where

$$\mathbf{Z}^{w} = (\varepsilon_{zx}, \varepsilon_{zy}), \quad \mathbf{Z}^{\varphi} = -(E_x, E_y), \quad \mathbf{Z}^{\psi} = -(H_x, H_y). \tag{4.7}$$

Putting (4.5) and (4.6) together, and recalling the constitutive relation (2.2) for the matrix, we obtain

Table 1
Material parameters of $BaTiO_3$, $CoFe_2O_4$ (Li & Dunn, 1998a), and Terfenol-D (Liu et al., 2003; Liu et al., 2004).

Property	$BaTiO_3$	$CoFe_2O_4$	Terfenol-D
$C_{44}(N/m^2)$	43×10^9	45.3×10^9	13.6×10^9
$e_{15}(C/m^2)$	11.6	0	0
$q_{15}(N/Am)$	0	550	108.3
$\kappa_{11}(C^2/Nm^2)$	11.2×10^{-9}	0.08×10^{-9}	0.05×10^{-9}
$\mu_{11}(Ns^2/C^2)$	5×10^{-6}	590×10^{-6}	5.4×10^{-6}
$\lambda_{11}(Ns/VC)$	0	0	0

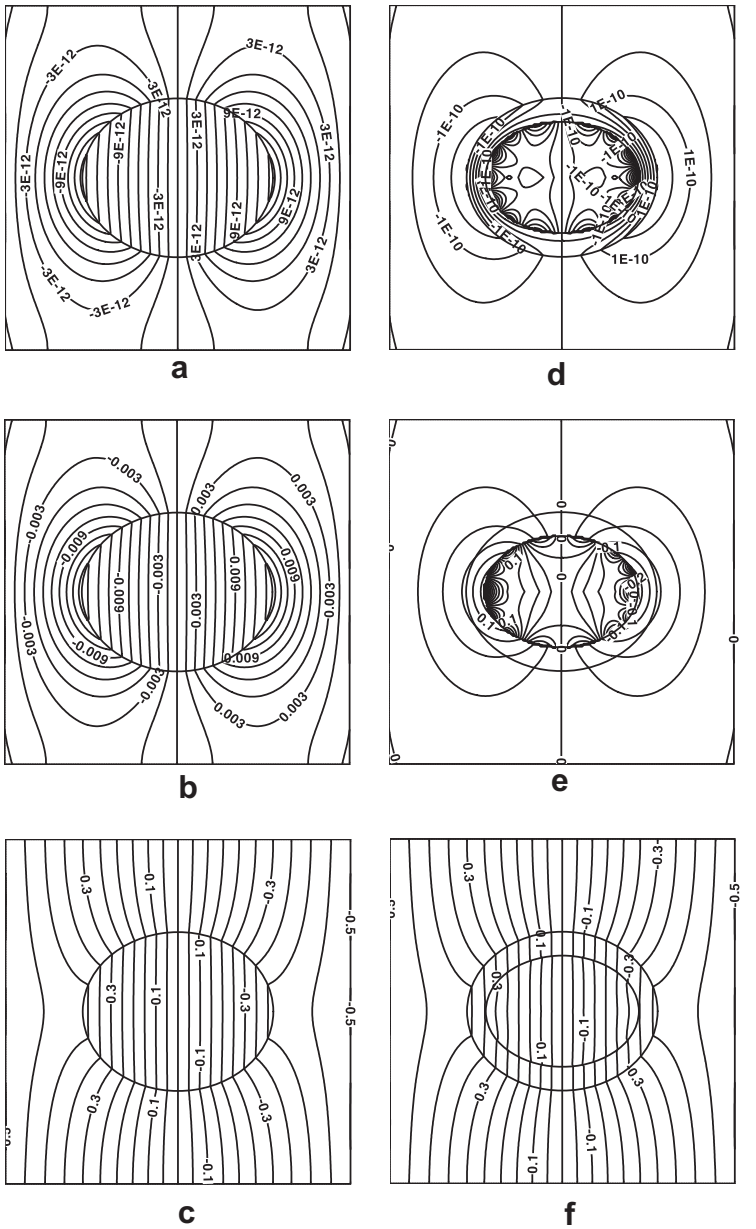

Fig. 3. Potential contours for a square array composite ($f = 0.2,\ \bar{\varepsilon}_{zx} = 0,\ \overline{E}_x = 0,\ \overline{H}_x = 1C/ms$) (a)–(c) BTO fibers embedded in a CFO matrix, (d)–(f) BTO fibers coated Terfenol-D embedded in a CFO matrix, (a), (d) Vertical displacement (m), (b), (e) Electric potential (V), (c), (f) Magnetic potential (C/s).

$$\begin{pmatrix} \langle \sigma_{zx} \rangle \\ \langle D_x \rangle \\ \langle B_x \rangle \end{pmatrix} = \begin{pmatrix} C_{44} & e_{15} & q_{15} \\ e_{15} & -\kappa_{11} & -\lambda_{11} \\ q_{15} & -\lambda_{11} & -\mu_{11} \end{pmatrix}^{(m)} \begin{pmatrix} \bar{\varepsilon}_{zx} - \frac{\pi d B_{1R}^{w}}{\alpha\beta} \\ -\overline{E}_x - \frac{\pi d B_{1R}^{\psi}}{\alpha\beta} \\ -\overline{H}_x - \frac{\pi d B_{1R}^{\psi}}{\alpha\beta} \end{pmatrix}. \tag{4.8}$$

Putting together (4.1) and (4.8) and noting that the coefficients B_{1R}^{Φ} depend linearly on the applied field I_R^{Φ}, we obtain set of equations for the effective property $\mathbf{L}_x^*$. We can determine this by applying different loading combinations between $\bar{\varepsilon}_{zx}$, $\overline{E}_x$ and $\overline{H}_x$. Similarly we can determine $\mathbf{L}_y^*$ by applying different loading combinations between $\bar{\varepsilon}_{zy}$, $\overline{E}_y$ and $\overline{H}_y$.

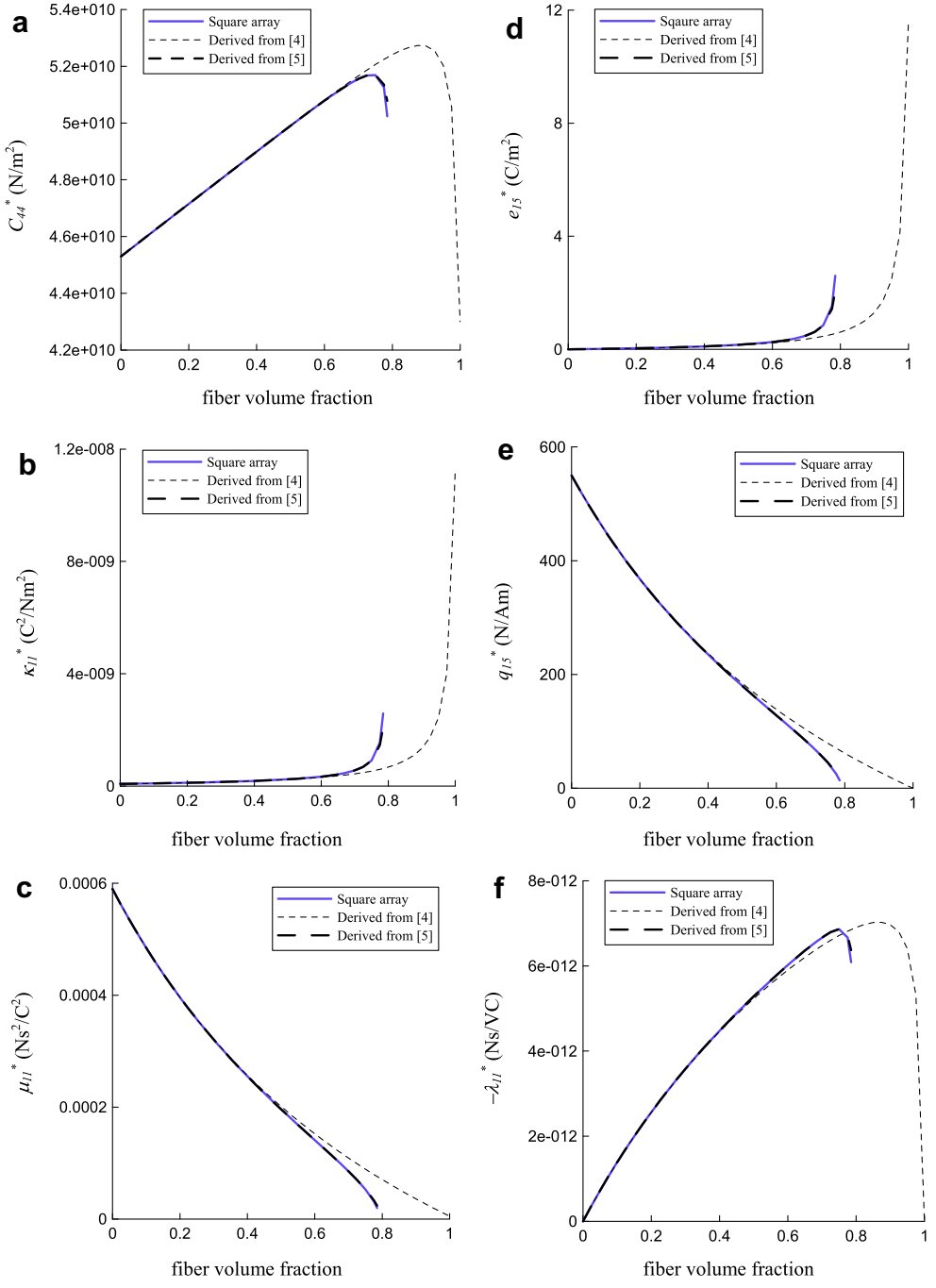

Fig. 4. Effective moduli of a composite of BTO fibers in a CFO matrix versus fiber volume fractions (a) effective elastic modulus, (b) effective dielectric permittivity, (c) effective magnetic permeability, (d) effective piezoelectric modulus, (e) effective piezomagnetic modulus, (f) effective magnetoelectric coefficient.

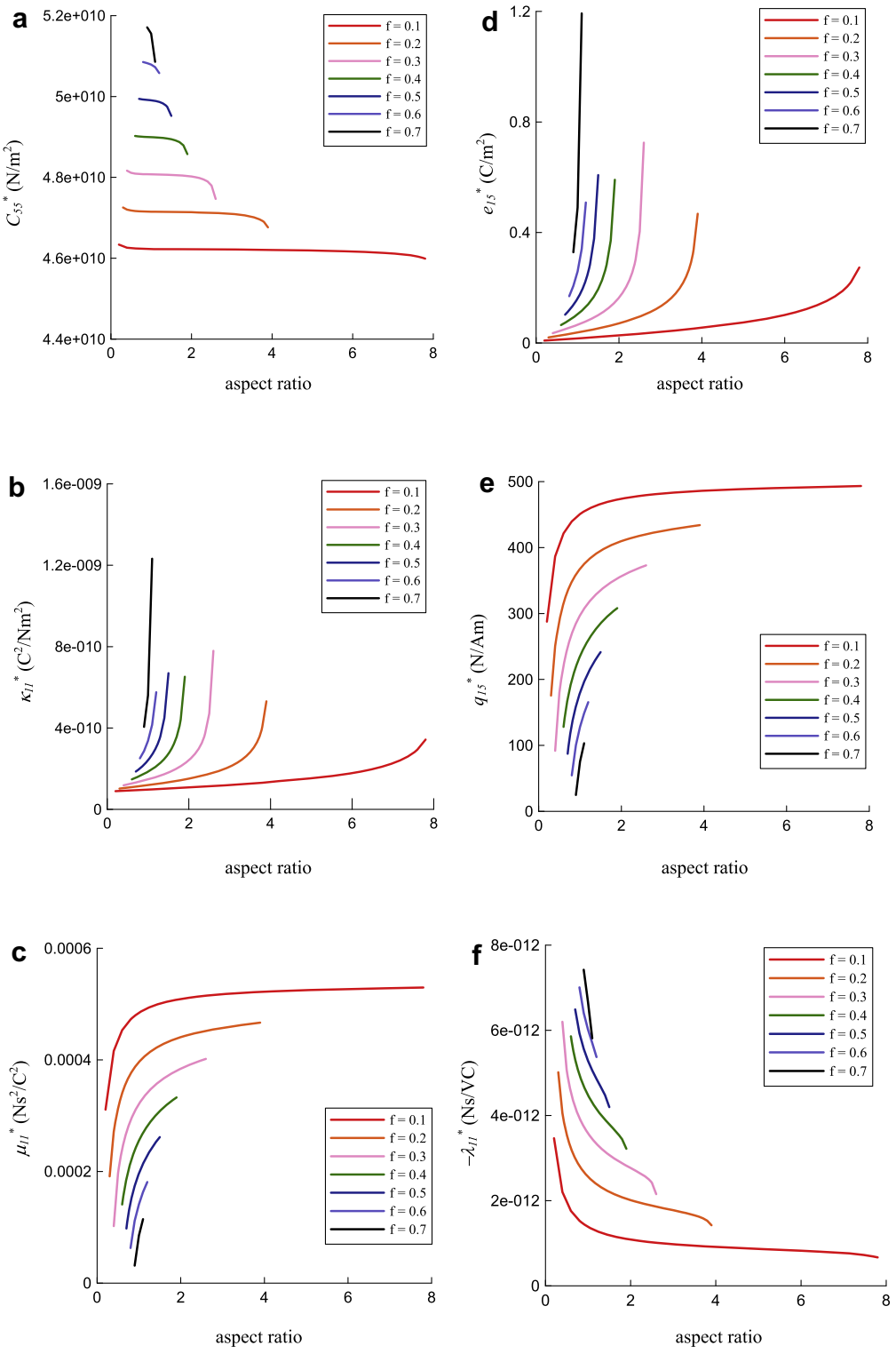

Fig. 5. Effective moduli of a composite of BTO fibers in a CFO matrix versus the aspect ratio and fiber volume fractions (a) effective elastic modulus, (b) effective dielectric permittivity, (c) effective magnetic permeability, (d) effective piezoelectric modulus, (e) effective piezomagnetic modulus, (f) effective magnetoelectric coefficient.

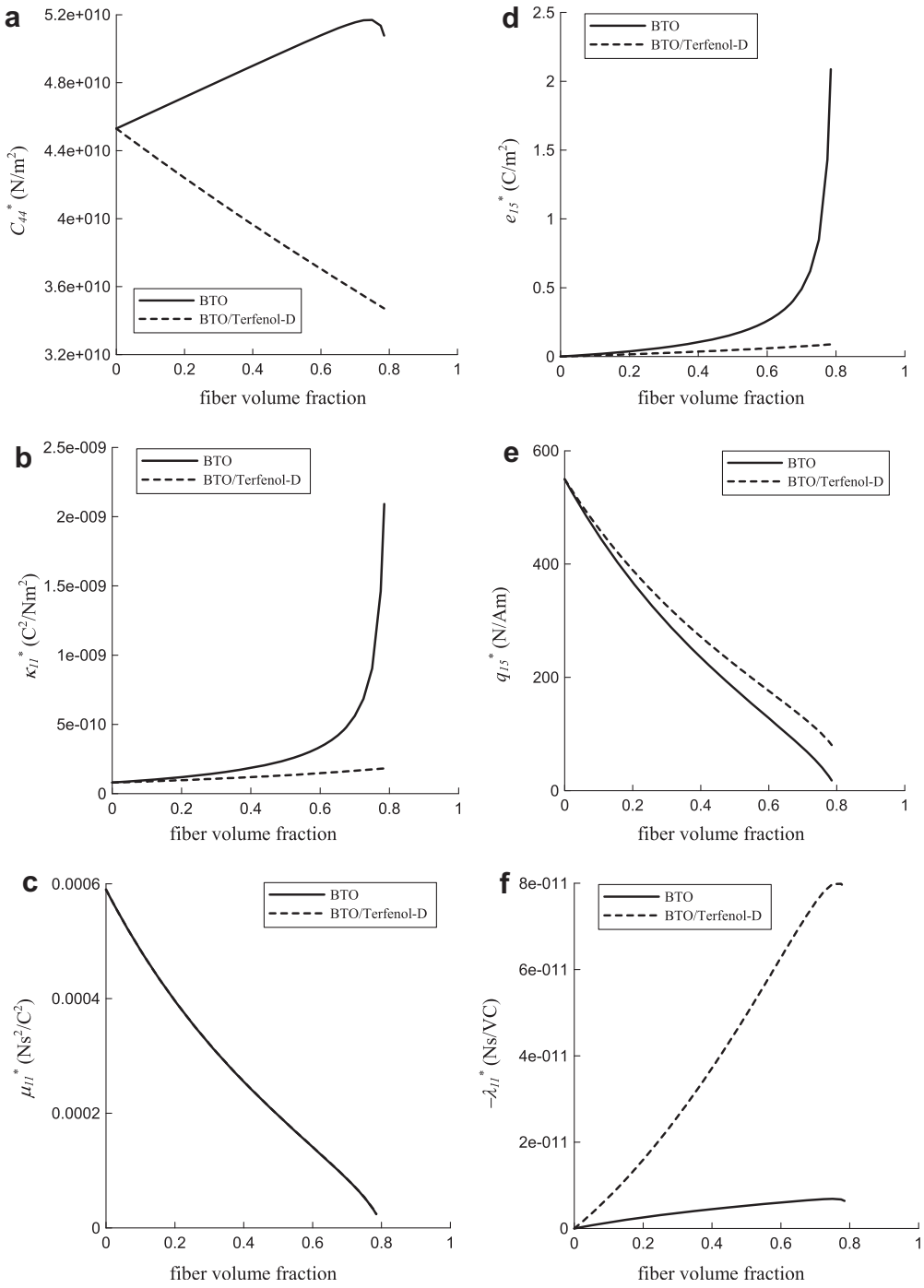

Fig. 6. Effective moduli of a composite of BTO fibers coated Terfenol-D in a CFO matrix versus fiber volume fractions (a) effective elastic modulus, (b) effective dielectric permittivity, (c) effective magnetic permeability, (d) effective piezoelectric modulus, (e) effective piezomagnetic modulus, (f) effective magnetoelectric coefficient.

5. Results and discussion

To have a better understanding for the theoretical results above, we perform a numerical computation for two- and three-phase transversely isotropic piezoelectric–piezomagnetic composites with 6 mm material symmetry about the fiber axis. For the piezoelectric material, we consider the widely used $BaTiO_3$ (BTO). For the peizomagnetic material, we consider $CoFe_2O_4$ (CFO) as well as the Terfenol-D alloy (TD). The cylinders are arranged in a square array. The independent material constants

of these constituents are given in Table 1, where the *xy* plane is isotropic and the fiber axis is along the *z*-direction. Note that in all materials magnetoelectric coefficients are zero, i.e. $\lambda_{11} = 0$.

We begin with a composite of BTO fibers in a CFO matrix. Fig. 3 (a–c) show the contours of displacement, electric potential and magnetic potential with an applied magnetic field. The ratio of the semi-axes l_x and l_y is 1.2. The magnetic field induces a mechanical stress in the CFO which in turn results in an electric displacement in the BTO fiber. The magnetic field is attracted by the BTO since it has a smaller magnetic permeability. Further, Fig. 3 (d–f) show the potential contours for BTO fibers coated TD in a CFO matrix with an applied magnetic field. The ratio of semi-axis l_x between BTO and TD is 0.7. Since the magnetic permeability of TD is almost the same as that of BTO, the magnetic potential is similar to its homogeneous counterpart. However, in this case the contours of vertical displacement and the electric potential have dramatically difference from those with the homogeneous fiber. The fields in the fiber are now not uniform, and there are field concentrations at the BTO and TD interfaces.

We now turn to effective moduli of the composite. Fig. 4 shows the effective elastic, dielectric, magnetic, piezoelectric, piezomagnetic and magnetoelectric moduli for this composite. We assume that the inclusions are circular cylinders, i.e., $l_x \to l_y$, and the inclusions are in a square array. Therefore there is no distinction between $\mathbf{L}_x^*$ and $\mathbf{L}_y^*$. The effective moduli vary nonlinearly with volume fraction, and the curve stops at $f = \frac{\pi}{4}$ when the inclusions touch. The magnetoelectric coefficient is non-zero for every non-zero volume fraction, then reaches a maximum before dropping just as the fibers are close to touching. Further, Fig. 4 also compares the effective moduli with those predicted by Benveniste (1995) who used the composite cylinder assemblage (CCA) model and by Camacho-Montes et al. (2009) who employed the asymptotic homogenization method. In CCA, there is no upper limit on the volume fraction since one can have fibers with various sizes. Still, the overall magnitudes and trends agree well among our periodic, Benveniste's CCA, and Camacho-Montes et al.'s homogenization method. In addition, our numerical results fulfil the compatibility conditions given in Eq. (21) of the work by Benveniste (1995).

Fig. 5 shows how the effective properties $\mathbf{L}_x^*$ of the composite depend on the fibers' aspect ratio l_x/l_y and volume fraction f. The value of the aspect ratio begins at $\frac{4f}{\pi}$ and terminates at $\frac{\pi}{4f}$ when the inclusions touch in y- and x-direction, respectively. It is observed that, for a fixed volume fraction, the effective elastic modulus and magnetoelectric coefficient decrease when the aspect ratio increases. While the effective dielectric permittivity, magnetic permeability, piezoelectric and piezomagnetic moduli increase monotonously. Furthermore, for a fixed aspect ratio, the effective elastic modulus, dielectric permittivity, piezoelectric, and magnetoelectric coefficients increase with increasing volume fraction, while the effective magnetic permeability and piezomagetic coefficient decrease when f increases. Interestingly, the trends of the dielectric permittivity and piezoelectric constant are similar, and those of the magneitc permeability and piezomagnetic coefficients are similar as well. In Fig. 6, we show the effective moduli for the BTO fibers coated TD in a CFO matrix. The ratio of the radius of BTO and TD is 0.8. We find that the magnetoelectric coefficient λ_{11}^* has dramatically enhanced, and the enhancement is increased as the particles touch.

We finally turn to the magnetoelectric voltage coefficient, which is the important figure of merit for magnetic field sensors. It relates the overall electric field that is generated in the composite when it is subjected to a magnetic field. It combines the coupling and dielectric coefficients, and is defined by

$$\alpha_{11}^* = \frac{\lambda_{11}^*}{\kappa_{11}^*}. \tag{5.1}$$

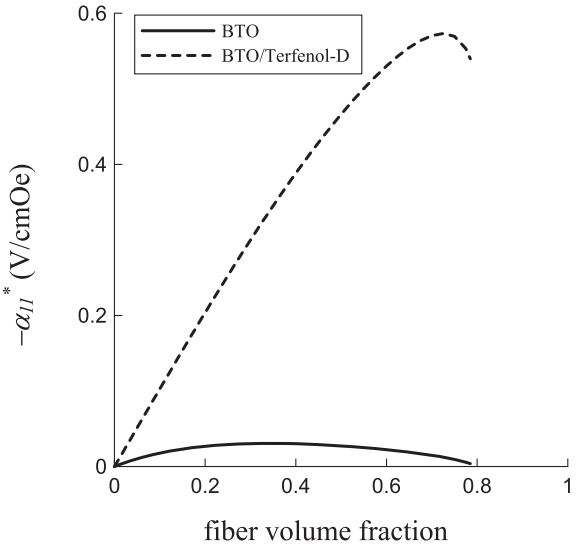

Fig. 7. Effective magnetoelectric voltage coefficient of the composite versus the fiber volume fraction.

Fig. 7 shows how this coefficient depends on the fiber volume fraction for the above two- and three-phase circular cylinder cases. Note that there is a qualitative difference between the case of BTO fibers in CFO and BTO fibers coated TD in the CFO matrix. In the former, the maximum coefficient is for intermediate volume fraction of $f = 0.35$ where $\alpha_{11}^{*} = 0.0306$ V/cmOe. In contrast, in the case of BTO fibers coated TD in the CFO matrix, the maximum is attained as the fibers near close touching at $f = 0.725$ where $\alpha_{11}^{*} = 0.5732$ V/cmOe, which is one order of magnitude enhancement of the coupling coefficient.

6. Concluding remarks

In summary, we have extended Rayleigh's formalism on periodic conductive composites to a magnetoelectroelastic composite consisting of arbitrarily distributed or periodic arrays of elliptic cylinders under anti-plane shear deformation, in-plane electric fields and in-plane magnetic intensities. The cylinders can be homogeneous or confocally multicoated. Expressions for the elastic, electric and magnetic potentials for the cylinders and the matrix are derived, and used to compute the effective moduli. This extension is a hybrid technique: the admissible potentials for the matrix and inclusions are expanded in complex planes, while the interface conditions are directly satisfied by using elliptic coordinates. It is shown that the effective properties solely depend on one particular constant B_{1R}^{Φ} among the infinite number of expansion coefficients. Finally, as a practical example, explicit numerical calculations for field distributions and the magnetoelectric effects in BTO-CFO and BTO-TD-CFO composites are presented and discussed. This example shows the important difference between the case of BTO fibers in a CFO matrix from the case of BTO fibers coated TD in a CFO matrix. We expect that these results will be beneficial as design tools for functionally graded tunable composites.

Acknowledgments

This work was supported by the National Science Council, Taiwan, under Contract No. NSC 98-2221-E-009-095.

References

Aboudi, J. (2001). Micromechanical analysis of fully coupled electro–magneto–thermo-elastic multiphase composites. *Smart Materials and Structures, 10*, 867–877.
Arfken, G. B., & Weber, H. J. (2001). *Mathematical methods for physicists*. San Diago: Academic Press. p. 62.
Astrov, D. N. (1960). The magnetoelectric effect in antiferromagnetics. *Soviet Physics JETP, 11*, 708–709.
Benveniste, Y. (1995). Magnetoelectric effect in fibrous composites with piezoelectric and piezomagnetic phases. *Physical Review B, 51*, 16424–16427.
Camacho-Montes, H., Sabina, F. J., Bravo-Castillero, J., Guinovart-Díaz, R., & Rodríguez-Ramos, R. (2009). Magnetoelectric coupling and cross-property connections in a square array of a binary composite. *International Journal of Engineering Science, 47*, 294–312.
Chen, T. Y. (1993). Piezoelectric properties of multiphase fibrous composites: Some theoretical results. *Journal of the Mechanics and Physics of Solids, 41*, 1781–1794.
Chen, W. Q., & Lee, K. Y. (2003). Alternative state space formulations for magnetoelectric thermoelasticity with transverse isotropy and the application to bending analysis of nonhomogeneous plates. *International Journal of Solids and Structures, 40*, 5689–5705.
Eerenstein, W., Mathur, N. D., & Scott, J. F. (2006). Multiferroic and magnetoelectric materials. *Nature, 442*, 759–765.
Harshé, G., Dougherty, J. P., & Newnham, R. E. (1993). Theoretical modelling of 3-0/0-3 magnetoelectric composites. *International Journal of Applied Electromagnetics in Materials, 4*, 161–171.
Huang, J. H. (1998). Analytical predictions for the magnetoelectric coupling in piezomagnetic materials reinforced by piezoelectric ellipsoidal inclusions. *Physical Review B, 58*, 12–15.
Huang, J. H., & Kuo, W.-S. (1997). The analysis of piezoelectric/piezomagnetic composite materials containing ellipsoidal inclusions. *Journal of Applied Physics, 81*, 1378–1386.
Kuo, H.-Y. (2010). Electrostatic interactions of arbitrarily dispersed multicoated elliptic cylinders. *International Journal of Engineering Science, 48*, 370–382.
Kuo, H. -Y., & Bhattacharya, K. (submitted for publication). Fibrous composites of piezoelectric and piezomagnetic phases.
Kuo, H.-Y., & Chen, T. (2008). Electrostatic fields of an infinite medium containing arbitrarily positioned coated cylinders. *International Journal of Engineering Science, 46*, 1157–1172.
Kushch, V. I., Shmegera, S. V., & Buryachenko, V. A. (2005). Interacting elliptic inclusions by the method of complex potentials. *International Journal of Solids and Structures, 42*, 5491–5512.
Landau, L. D., & Lifshitz, E. M. (1984). *Electrodynamics of continuous media*. New York: Pergamon Press. p. 119.
Li, J. Y. (2000). Magnetoelectroelastic multi-inclusion and inhomogeneity problems and their applications in composite materials. *International Journal of Engineering Science, 38*, 1993–2001.
Li, J. Y., & Dunn, M. L. (1998a). Micromechanics of magnetoelectroelastic composite materials: Average fields and effective behaviour. *Journal of Intelligent Material Systems and Structures, 9*, 404–416.
Li, J. Y., & Dunn, M. L. (1998b). Anisotropic coupled-field inclusion and inhomogeneity problems. *Philosophical Magazine A, 77*, 1341–1350.
Liu, G., Nan, C.-W., Cai, N., & Lin, Y. (2004). Dependence of giant magnetoelectric effect on interfacial bonding for multiferroic laminate composites of rare-earth-iron alloys and lead–zirconate–titanate. *Journal of Applied Physics, 95*, 2660–2664.
Liu, Y. X., Wan, J. G., Liu, J.-M., & Wen, C. W. (2003). Numerical modeling of magnetoelectric effect in composite structure. *Journal of Applied Physics, 94*, 5111–5117.
Milgrom, M., & Shtrikman, S. (1989). Linear response of two-phase composites with cross moduli: Exact universal relations. *Physical Review A, 40*, 1568–1575.
Nan, C.-W. (1994). Magnetoelectric effect in composites of piezoelectric and piezomagnetic phases. *Physical Review B, 50*, 6082–6088.
Nan, C.-W., Bichurin, M. I., Dong, S., Viehland, D., & Srinivasan, G. (2008). Multiferroic magnetoelectric composites: Historical perspective, status, and future directions. *Journal of Applied Physics, 103*, 031101.
Nicrovici, N. A., & McPhedran, R. C. (1996). Transport properties of arrays of elliptical cylinders. *Physical Review E, 54*, 1945–1957.
Pan, E., & Han, F. (2005). Exact solution for functionally graded and layered magneto–electro-elastic plates. *International Journal of Engineering Science, 43*, 321–339.
Petrov, V. M., & Srinivasan, G. (2008). Enhancement of magnetoelectric coupling in functionally graded ferroelectric and ferromagnetic bilayers. *Physical Review B, 78*, 184421.

Petrov, V. M., Srinivasan, G., & Galkina, T. A. (2008). Microwave magnetoelectric effects in bilayers of single crystal ferrite and functionally graded piezoelectric. *Journal of Applied Physics, 104*, 113910.

Rado, G. T., & Folen, V. J. (1961). Observation of the magnetically induced magnetoelectric effect and evidence for antiferromagnetic domains. *Physical Review Letters, 7*, 310–311.

Rayleigh, L. (1892). On the influence of obstacles arranged in rectangular order upon the properties of a medium. *Philosophical Magazine, 34*, 481–502.

Srinivas, S., Li, J. Y., Zhou, Y. C., & Soh, A. K. (2006). The effective magnetoelectroelastic moduli of matrix-based multiferroic composites. *Journal of Applied Physics, 99*, 043905.

Suresh, S. (2001). Graded materials for resistance to contact deformation and damage. *Science, 292*, 2447–2451.

Wang, X., Pan, E., Albrecht, J. D., & Feng, W. J. (2009). Effective properties of multilayered functionally graded multiferroic composites. *Composite Structures, 87*, 206–214.

Wu, T.-L., & Huang, J.-H. (2000). Closed-form solutions for the magnetoelectric coupling coefficients in fibrous composites with piezoelectric and piezomagnetic phases. *International Journal of Solids and Structures, 37*, 2981–3009.